# Low-Profile Enhanced-Bandwidth PIFA Antennas for Wireless Communications Packaging

Kathleen L. Virga, *Senior Member, IEEE,* and Yahya Rahmat-Samii, *Fellow, IEEE*

***Abstract*—The development of small integrated antennas plays a significant role in the progress of the rapidly expanding military and commercial communications applications. The recent advances in RF and microwave high-density circuit packaging technologies in multifunction wireless communications systems have called for the parallel development of compact and efficient antennas that can be used over a wide frequency range. This paper addresses the development and characterization of several low-profile and integrated antennas with enhanced bandwidth for wireless communications systems. The new radiators are developed by adding parasitic elements or tuning devices to a familiar integrated antenna—the planar inverted F antenna (PIFA). Simulations based upon the finite-difference time-domain (FDTD) method and method of moments (MoM) are used to model the performance of the antennas. Comparisons with measured results on fabricated antenna structures are provided for simulations validation.**

***Index Terms*— Broad-band antennas, conformal antennas, FDTD, MoM, PIFA, wireless communications.**

## I. Introduction

THE RAPID progress in wireless communications promises to make interactive voice, data, and video services available anytime and anyplace. The technology to support these applications has been made possible by recent advances in high-density RF and microwave circuit packaging. Wireless communications systems come in a variety of different sizes ranging from small hand-held devices to backpack-style "man-pack" radio units to wireless local area networks to devices mounted on vehicles. The current focus in electronics packaging and interconnects has led to the development of low-cost multichip modules and circuitry that can readily be incorporated into a broad spectrum of systems. For optimum system performance, the antennas must also have high radiation efficiency, small volume, isotropic radiation characteristics, simple and low-loss impedance matching to the receive and transmit paths, and simple mechanical construction.

In order to determine the appropriate antenna to use, it is necessary to evaluate the electrical and mechanical characteristics and to assess how the antenna will be situated with respect to the overall wireless system package. Simulations based upon either the finite-difference time-domain (FDTD) method [1]-[2] or surface-patch method of moments (MoM) [3] are good analysis approaches to use to assess the applicability of diverse types of antenna elements. The FDTD and MoM design tools are used to critically evaluate the performance of enhanced bandwidth radiators.

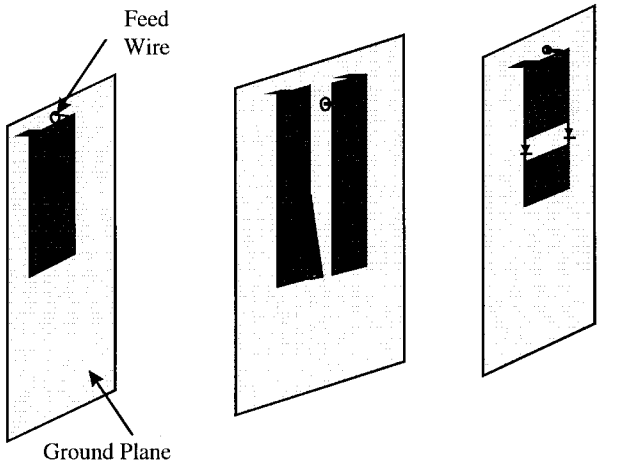


Fig. 1. Low-profile integrated antenna configurations for wireless communications applications.

Fig. 1 shows the configurations of several low-profile antennas with enhanced bandwidth performance. These antennas include the radiation-coupled Dual L antenna (Dual L) [4], [5] and the diode-tunable planar inverted F (diode PIFA) antennas. These antenna structures have specific advantages over other candidate elements because the bandwidth is increased while maintaining a low-profile geometry and without additional internal matching networks. In this paper, the results of an in-depth PIFA study are used to develop enhanced bandwidth low-profile antenna elements. The influence of the different antenna components on performance is characterized. Prototype elements have been fabricated and tested in order to validate the numerical models and design approach.

Part of this paper concentrates on the unique visualization of the surface currents on the antennas. Surface current plots can be used to understand the electromagnetic behavior of intricate antenna structures radiating in a complex environment. They provide insight into the radiation mechanisms of the antennas and give a snapshot of the interactions between the antenna and wireless package.

Section II discusses the FDTD and MoM simulation approaches employed to develop the antennas in this paper.

Manuscript received January 5, 1997; revised May 19, 1997. This work was supported in part by Rockwell Science Center, Thousand Oaks, CA, and in part by the UC MICRO Program.

K. L. Virga is with the Department of Electrical and Computer Engineering, University of Arizona, Tucson, AZ 85721-0104 USA.

Y. Rahmat-Samii is with the University of California, Los Angeles, Los Angeles, CA 90095-1594 USA.

Publisher Item Identifier S 0018-9480(97)07397-3.

The development and characterization of integrated antenna elements are presented in Section III. In the first part of this section, a detailed study of the behavior of the PIFA is discussed. The results in this part are used to modify the antenna element in order to enhance its bandwidth performance. The design and development of the Dual L and diode PIFA antennas are then presented. Plots of the surface currents on the Dual L are used to explain the radiation characteristics of this antenna. Section IV provides concluding remarks and discusses the application and integration of these antennas into future wireless systems.

## II. Simulation Methodologies

An important task associated with the evaluation and comparison of different antenna configurations involves the appropriate application of simulation tools capable of accurately predicting antenna performance in the mobile environment. Such tools must adequately characterize and analyze the radiation characteristics as well as the input impedance of many geometrically diverse antennas. In addition to tradeoff comparisons, accurate simulations may be used to develop design curves for novel radiators, optimize the antenna designs, and perform sensitivity analyses.

Algorithms based upon the FDTD method and surface patch MoM are capable of predicting the electromagnetic behavior of intricate antenna structures radiating in a complex environment. The FDTD method and MoM each have specific advantages and disadvantages, thus the availability of both approaches allows for the analysis of diverse types of antennas. The FDTD method is based upon the explicit solution of Maxwell's equations in differential form in the time domain. The radiation pattern for an antenna is obtained by computing and storing the tangential time-domain fields over a surface which completely encloses the antenna using FDTD, and subsequently using the equivalence principle to determine the field values in the far-zone.

The MoM approach is based upon a numerical solution of the electric field integral equation imposed at perfect electric conducting surfaces to determine the surface currents, and thus, the radiation characteristics. The application of efficient numerical techniques, such as the one described in [6], can be employed to reduce the time it takes to perform MoM simulations over many frequencies. The surface patch MoM approach uses a triangular surface mesh of the radiator. In the past, some antenna designers have used the wire-grid MoM approach because of its convenience to describe antenna geometries and its ability to run on personal computers. However, wire-grid modeling of solid flat surfaces has several inherent problems. The far-field results are generally acceptable, but near-field results, such as input impedance or the current distribution on an antenna attached to a complex metal body, are often inaccurate [7], [8]. There are additional MoM-based approaches that can be applied to the solution of antennas for integrated wireless packaging design. One method that models dielectric objects in the vicinity of the antenna and wireless package is based upon a volume integral equation solution approach [9]. Another method, described in [10], incorporates a hybrid MoM/physical-optics technique that allows for the efficient solution of large and complex packaged structures.

## III. Characterization of Integrated Antennas

This section presents the results of the development of several compact broad-band radiators suitable for wireless communications. The particular configurations to be investigated have several unique features that make them especially useful for various packaged wireless systems. All of the structures are low profile, which results in unobtrusive antenna elements that are resistant to breakage and a wireless system with an overall low-profile form factor. The antennas are simple to manufacture, have simple coax feeds, and employ minimal use of dielectric materials, which typically introduce material losses and thus reduce the overall antenna efficiency.

Several different definitions are typically used to characterize antenna bandwidth. Generally, a distinction between pattern bandwidth and impedance bandwidth is made. The focus of this paper will be on improving the impedance bandwidth of the antenna. The values will be specified as the frequency bandwidth in which the voltage standing-wave ratio (VSWR) is less than 2:1. A 2:1 VSWR is equivalent to a 10-dB return loss, the level at which 10% of the incident power is reflected back to the source.

In the first part of this section, the effect on input impedance due to changes in key parameters of the PIFA is discussed. A comparison of the performance of the PIFA computed by the FDTD method, MoM, and measurements is given. In the remaining parts of this section, the PIFA is modified in ways that extend the maximum bandwidth obtainable from this element. In the case of the Dual L, an additional coupled element is added to the PIFA structure. In the case of the diode PIFA, tuning diodes are added to effectively tune the length of the PIFA element. The addition of diodes to the PIFA structure overcomes some of fundamental limitations that exist in the general problem of matching an arbitrary load impedance to a pure resistance [11], [12].

### *A. Planar Inverted F Antenna (PIFA)*

This section describes the design of planar inverted F antennas (PIFA's). It summarizes the results of a series of simulations used to investigate how the different physical parts of the PIFA affect the input impedance, bandwidth, and resonant frequency of the antenna. The results of this study can be used to develop a design methodology to design PIFA's for operation at a defined frequency range. The results also give insight on how the PIFA may be modified in order to achieve wider bandwidth.

The PIFA consists of a ground plane, a top plate element, a feed wire attached between the ground plane and the top plate, and a shorting wire or strip that is connected between the ground plane and top plate. The antenna is fed at the base of the feed wire at the point where the wire connects to the ground plane. The effects of the ground plane (or wireless package) and the different parts of the antenna must be considered in the overall design. The PIFA is an attractive antenna for wireless systems where the space volume of the antenna is quite limited.

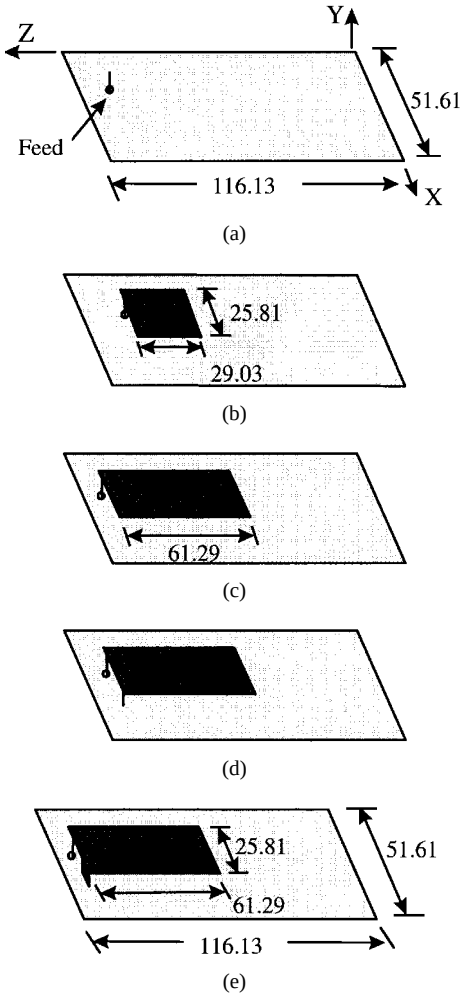


Fig. 2. Geometry configurations of PIFA in different stages of construction. All dimensions are in millimeters. (a) Feed wire on a ground plane. (b) Feed wire and short top plate. (c) Feed wire and full-length top plate. (d) PIFA with shorting wire. (e) PIFA with shorting strip.

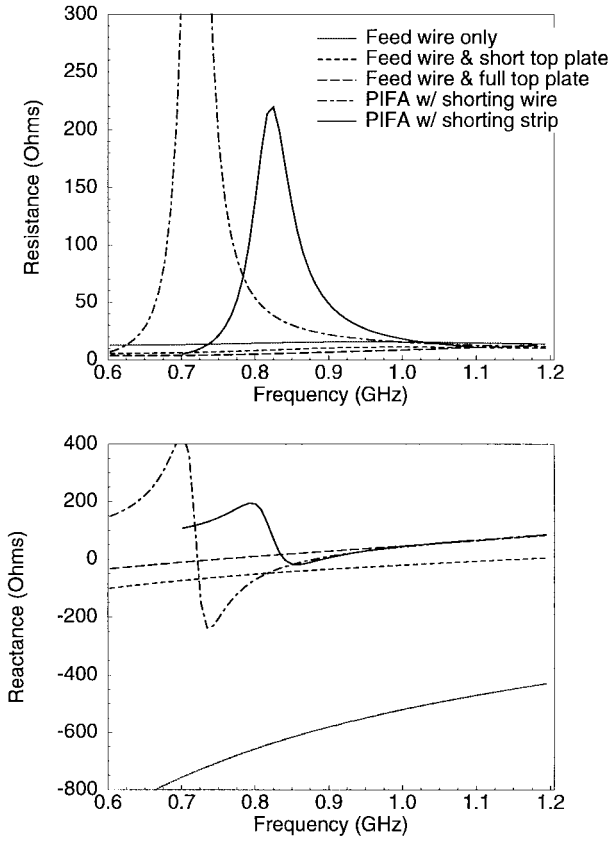


Fig. 3. Impedance characteristics for the PIFA in different stages of construction.

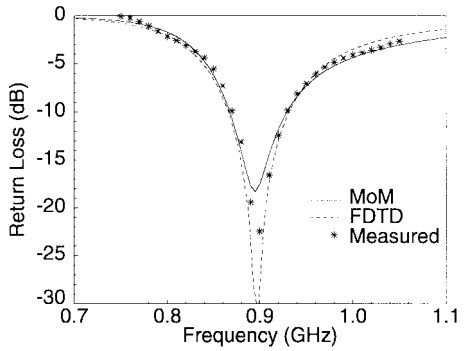


Fig. 4. Comparison of the FDTD method, MoM, and measured return loss for PIFA in Fig. 2(e).

It requires simple manufacturing, since the radiator must only be printed. The addition of the shorting strip allows good impedance match to be achieved with a top plate that is typically less than $\lambda/4$ long. The resulting PIFA is more compact than a conventional half-wavelength probe-fed patch antenna.

The design variables for this antenna are the height, width, and length of the top plate, the width and location of the shorting plate, and the location of the feed wire. A difficult task in the design of antennas that have many different design variables is the determination of the dimensions in order to obtain a specified input impedance at the center design frequency. A description of some of the design parameters which affect the resonant frequency and the bandwidth of the PIFA is given in [13]. This reference identifies the antenna height as the dominant factor which determines the bandwidth. However, little guidance is given on how to use this information to design a PIFA and how the variation of the physical parameters yields a particular PIFA design.

In order to identify the effect on input impedance of each part of the PIFA, a study of the PIFA in different stages of construction was performed. The input impedance was computed for the five different configurations shown in Fig. 2. The dimensions were determined so that the resulting PIFA shown in Fig. 2(e) will have 50-$\Omega$ input impedance at 0.90 GHz. The height of the PIFA is 12.90 mm, and the top plate of the PIFA is approximately 0.18 $\lambda$ long. The specific dimensions conform to a unit FDTD cell that is approximately a 3.23-mm-square cube to allow for an accurate comparison between FDTD and MoM simulations. The "feed wire only" geometry in Fig. 2(a) consists of a 12.90-mm-high feed wire mounted on a ground plane, which represents a side of the wireless package. The "feed wire and short top plate" configuration is shown in Fig. 2(b). The top plate in this case is about 0.09 $\lambda$ long. The "feed wire and full top plate" configuration in Fig. 2(c) is obtained by extending the length

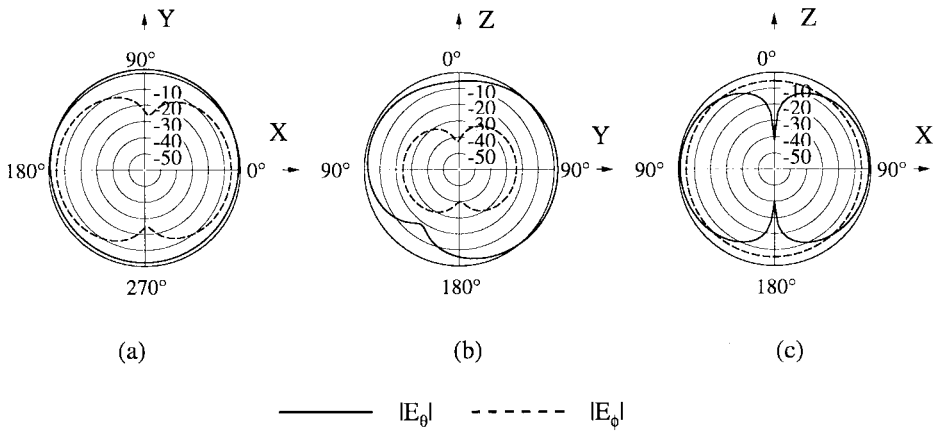


Fig. 5. Directivity patterns of PIFA in Fig. 2(e) at 0.90 GHz for various far-field components. (a) $|E|$ dB versus $\phi$, $\theta = 90°$, (b) $|E|$ dB versus $\theta$, $\phi = 90°$, (c) $|E|$ dB versus $\theta$, $\phi = 0°$.

of the top plate in Fig. 2(b) to 0.18$\lambda$. The "PIFA with shorting wire" in Fig. 2(d) is obtained by adding a shorting wire to the configuration shown in Fig. 2(c). The "PIFA with shorting strip" in Fig. 2(e) is obtained by replacing the shorting wire with a shorting strip.

The input impedance of each of these different configurations is plotted in Fig. 3. The resistance of the "feed wire only" is low and the reactance is strongly capacitive. This is characteristic of electrically small monopoles and dipoles. The reactance of the "feed wire and short top plate" configuration is much less capacitive than the "feed wire only" structure. The decrease in capacitance is obtained by increasing the effective length and thus, the inductance of the feed wire by the addition of the top plate. Extending the length of the top plate adds even more inductance to the structure as exhibited by the "feed wire and full top plate" structure. The resistance of the structures with the short- and full-length top plate is also quite low. These results show that the length and height of the top plate determine the reactance of the element, and thus, the resonant frequency.

The "PIFA with shorting wire" configuration has strong antiresonance characteristics. The impedance at the antiresonance has a sharp peak in the resistance and a sharp swing in the reactance from highly inductive to highly capacitive. The resistance for the antenna without the short wire is very low. The impedance for the antenna with the short wire peaks up to more than 300 $\Omega$ at the antiresonance and drops to nearly 10 $\Omega$ after the antiresonance. Control of the characteristics of the antiresonance is accomplished by replacing the short wire with a short strip, as shown in the impedance of the PIFA. A purely real 50-$\Omega$ input impedance is obtained at the frequency where the reactance is zero and the resistance drops to 50 $\Omega$. The input impedance for the configurations which have the full-length top plate shown in Fig. 2(c)–(e) is the same for the frequencies above 0.98 GHz. The length of the top plate and the location of the feed wire with respect to the shorting plate both determine the resonant frequency and overall bandwidth of the PIFA. The best bandwidth obtained for the PIFA is 9.61%.

A PIFA based upon the dimensions shown in Fig. 2(e) was fabricated and measured. The PIFA was constructed by cutting out the top plate, short plate, and ground plane conductors from thin sheets of copper-clad Duroid material. The antenna was assembled by soldering together the individual pieces to form the PIFA structure. A semirigid coax with a center conductor that extends 12.90 mm beyond the end of the outer conductor was used to form the PIFA feed wire. The outer conductor of the coax was soldered to the edge of a small hole drilled in the ground plane at the specified feed point. Note that in Fig. 2(e), the feed is flush with the top edge of the top plate, and is 12.90 mm from the edge of the top plate. The return loss of the antenna was measured on an HP8510C vector network analyzer using a one-port short-open-load calibration.

Fig. 4 compares the return loss for the PIFA in Fig. 2(e) computed by the FDTD and MoM programs developed at the University of California at Los Angeles (UCLA), and by measurement. The FDTD and MoM computed return loss agree well with measurements. The measurements and both simulation approaches predict the same bandwidth and center frequency. This comparison validates the FDTD and MoM computer models, and ensures that the associated grid and mesh sizes are small enough to obtain convergence in the numerical simulations.

The far-field directivity patterns of the PIFA in Fig. 2(e) computed by MoM are shown in Fig. 5. The patterns computed by FDTD are identical to the patterns in Fig. 5. The PIFA coordinate orientation information is shown in Fig. 2. The directivity is computed using the antenna input voltage and current. The far-field patterns predicted by FDTD and MoM have been validated by comparing the patterns computed for a monopole antenna on a box with measured results presented in [14].

The PIFA is linearly polarized with the desired broad radiation pattern. Fig. 5(a) and (c) show both high $E_\theta$ and $E_\phi$ components. The $z$-component of surface currents contribute to the $E_\theta$ far-field pattern in the $Y$- and $X$-directions. The $y$-component of surface current on the feed wire and the shorting strip contributes to the $E_\phi$ pattern in the $X$-direction and the $E_\theta$ pattern in the $Z$-direction for $\phi = 90°$. The $x$-component of current contributes to the $E_\phi$ pattern in the $Y$-direction and the $E_\theta$ pattern in the $Z$-direction for $\phi = 0°$. The pattern contribution of the $z$- and $y$-components of current are more significant than the pattern contributions from the $x$-component of current.

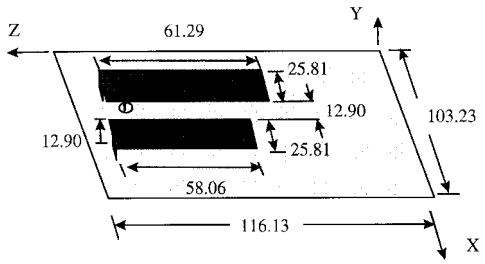


Fig. 6. Dimensions of Dual-L antenna. All dimensions are in millimeters.

The characteristics of these radiation patterns can be significantly affected in the presence of the particular wireless package [15], therefore, the environment of the packaged antenna design must be completely characterized. The objective of this paper is to identify some suitable antenna candidates to consider for the overall development of wireless systems and packages. The design of specific antennas for all types of wireless systems is especially difficult since the associated package designs can range from large basestation units to wireless handsets. Some simulations on the effects of narrowing or shortening the ground place were conducted. Narrowing the ground plane has a greater effect on the input impedance than does shortening the end of the ground plane. This is expected, since the currents that flow in the $z$-direction parallel to the sides of the ground plane are larger than the currents that flow in the $z$-direction normal to the end of the ground plane opposite the short plate and feed.

To improve the bandwidth of small antennas, loading is often used. Loading can be done with additional conductors or with resistive, inductive, and capacitive components. The use of additional conductors provides more physical parameters to vary in order to tailor the low- and high-frequency characteristics of the antenna design. Loading the antenna with variable resistive, inductive, or capacitive components allows the antenna to be tuned to multiple frequencies.

### *B. Enhanced Bandwidth Radiation-Coupled Dual Inverted L Antenna*

The Dual L antenna is principally a PIFA with a second element that consists of a top plate and short strip. This second element is radiation coupled (rather than directly fed) to the main element. The elements are arranged in parallel with a narrow slot in between them. The two metal top plates form the so-called inverted "L's" on the ground plane. The Dual L antenna structure is shown in Fig. 6. Each top plate element has a shorting strip that connects the plate to the mounting ground plane, but only the main-fed element has a feed wire. The Dual L antenna can be designed to have two principal resonant frequencies. The dimensions of the main-fed element are designed for 50-$\Omega$ input impedance at one frequency, while the dimensions of the composite configuration with the second element are designed for a 50-$\Omega$ match at another frequency. The overall bandwidth is increased when the two frequencies are brought close to each other. This results in an overall bandwidth that is a combination of the individual resonances—similar to what is observed in an overcoupled filter response. This increased bandwidth is accomplished without additional external matching circuits.

The Dual L has more than twice the number of design parameters of the PIFA. The design parameters for the Dual L are:

a) height of both elements over ground plane;
b) width of main-fed element;
c) length of main-fed element;
d) width of shorting strip on main-fed element;
e) location of feed wire;
f) gap between main and coupled element;
g) width of coupled element;
h) length of coupled element;
i) width of shorting strip on coupled element.

The four dominant parameters which determine the bandwidth of the Dual L antenna have been determined experimentally in [4]. This reference cites that the antenna height and the width of the gap between the main and coupled element are the dominant factors that control the bandwidth. This information was used to study the design and performance of the Dual L and to develop a methodology to design Dual L antennas to operate for any frequency.

The effects of several of the geometrical parameters on the input impedance and the bandwidth were studied. Simulations based upon FDTD and MoM were used to study the effects of several of the geometrical parameters on the input match and bandwidth. The starting design for the Dual L antenna is a main-fed element with the dimensions of the PIFA in Fig. 2(e) and a coupled element with similar dimensions. The design parameters that were varied were the gapwidth, the feed location, and the length and width of the coupled element.

The percentage bandwidth is the difference between the upper and lower frequencies for which the return loss is below $-10$ dB divided by the average of the upper and lower frequencies. Both the input impedance and the return loss are considered in this investigation. The impedance gives information on how the element must be modified (i.e., by adding capacitive or inductive reactance) to achieve a specified resonance frequency, while the return loss indicates how well the antenna is matched to the communication system.

Fig. 7 shows the input impedance and return loss as a function of the gapwidth. The feed is placed in the top corner of the main-fed element. When the gap is narrow, the two top plate elements function as if they were one large element. When the gap is large, there is little coupling between the main and parasitic elements, and the antenna behaves like an isolated PIFA. The curves show that the width of the gap controls the location of the first resonance and the interaction between the two resonances. When the gap is 9.68 mm wide, the resistance between the two resonances dips to nearly 35 $\Omega$. When the gap is 12.90 mm wide, the resistance dips to 60 $\Omega$. The return loss in each of the 9.68- and 12.90-mm-wide gap cases shows two closely spaced frequencies where the antenna is well matched. For frequencies above 0.92 GHz, the impedance of each of the configurations is the same as the impedance of an isolated PIFA. The second element primarily affects the impedance below 0.90 GHz.

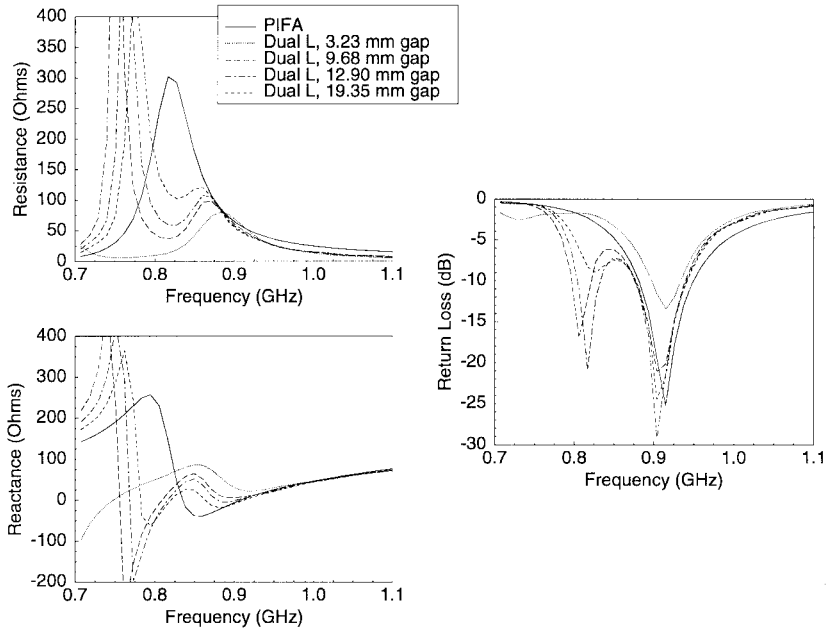


Fig. 7. Input impedance and return loss versus gapwidth for Dual L antenna. Feed is located at top corner of main element. (a) Input impedance. (b) Return loss.

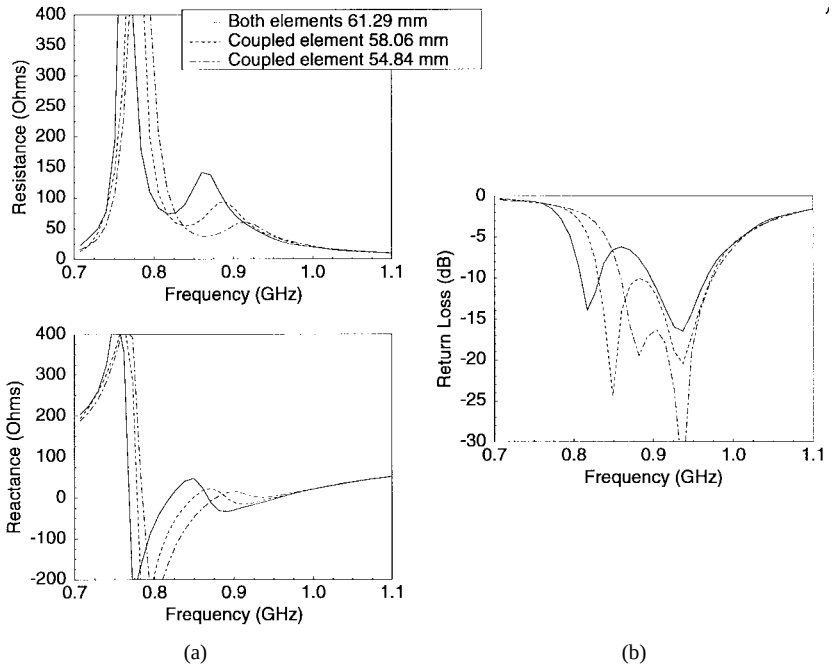


Fig. 8. Input impedance and return loss versus coupled element length for Dual L with 12.90-mm gap. Feed is located 6.45 mm from top. (a) Input impedance. (b) Return loss.

The location of the feed on the main element is one factor that controls the frequency, bandwidth, and minimum return loss of the upper resonance. The widest bandwidth of the PIFA in Fig. 2(e) is obtained when the feed is 6.45 mm from the top of the main element. Similar simulations on the Dual L antenna showed that a bandwidth improvement was achieved by moving the feed away from the top corner of the main-fed element. Thus, in the remaining results the feed is located 6.45 mm away from the top corner and along the side edge of the main-fed element that is closest to the coupled element.

The effect of the length of the coupled element is shown in Fig. 8. The gap between the main-fed and coupled elements is 12.90 mm. These curves show that length of the coupled element controls the resistance and reactance between the two resonances to achieve an overall broad-bandwidth. The 58.06-mm-long coupled element yields 16.06% bandwidth, while the 54.84-mm-long coupled element yields only 12.84% bandwidth. The effects of the width of the coupled element are shown in Fig. 9. The gap between the main-fed and coupled elements is 12.90 mm wide, and both elements are 61.29

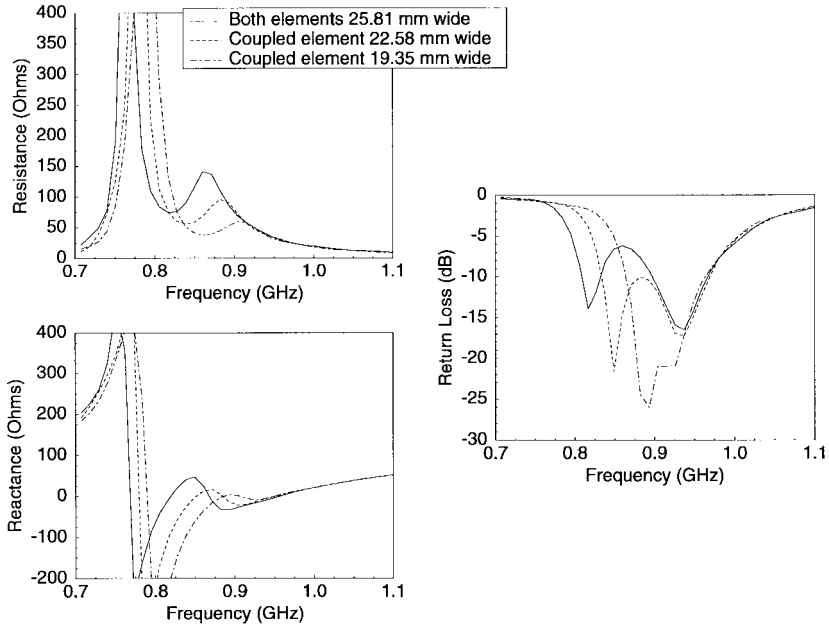


Fig. 9. Input impedance and return loss versus coupled-element width for Dual L with 12.90-mm gap. Feed is located 6.45 mm from top. (a) Input impedance. (b) Return loss.

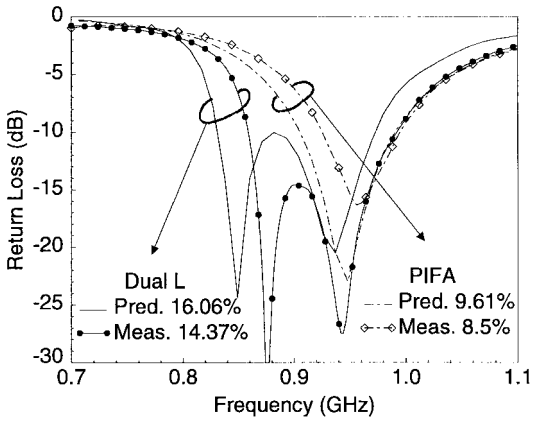


Fig. 10. Comparison of predicted and measured return loss and percent bandwidth for PIFA and Dual L antennas.

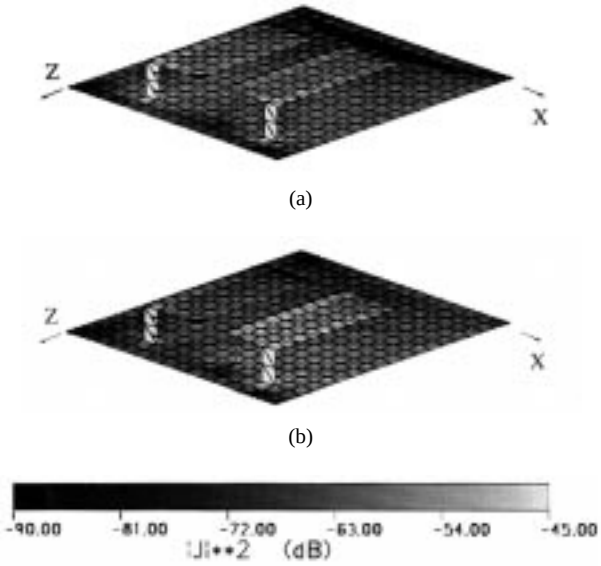


Fig. 11. Magnitude of surface currents of Dual L antenna. (a) 0.84 Ghz. (b) 0.94 GHz.

mm long. The curves indicate that the element width has a similar influence on the bandwidth as does the element length. The 22.58-mm-wide coupled element yields 15.41% bandwidth, while the 19.35-mm-wide coupled element yields 11.32% bandwidth. Simulations of varying the length and width of the coupled element using a 9.68-mm gap between the main-fed and coupled elements had the same effect, but did not produce as wide bandwidth as did the Dual L with the 12.90-mm gapwidth.

Based upon the results of these simulations, a Dual L antenna was fabricated from the dimensions specified in Fig. 6. The antenna was fabricated in a manner similar to the method used for the fabrication of the PIFA. The return loss was measured using an HP8510C. Fig. 10 compares the predicted and measured return loss of both the PIFA and Dual L antennas. The PIFA results were obtained from taking the larger ground plane of the Dual L antenna and determining the return loss of the isolated main-fed element. The Dual L results were obtained by adding the coupled element to the structure. There is good agreement between the measured and predicted return loss. The Dual L has nearly twice the bandwidth of the PIFA. The measured results are shifted slightly higher in frequency than the predicted results. This is due to small differences between the location of the feed and the gapwidth in the fabricated antenna and in the simulations. Some additional tests showed that the lower resonant frequency can be shifted by a slight repositioning of the coupled element and adjusting the gapwidth. Detailed studies on the isolated PIFA element indicate that the placement of the feed is the dominant factor that controls the resonant frequency for a given size top plate.

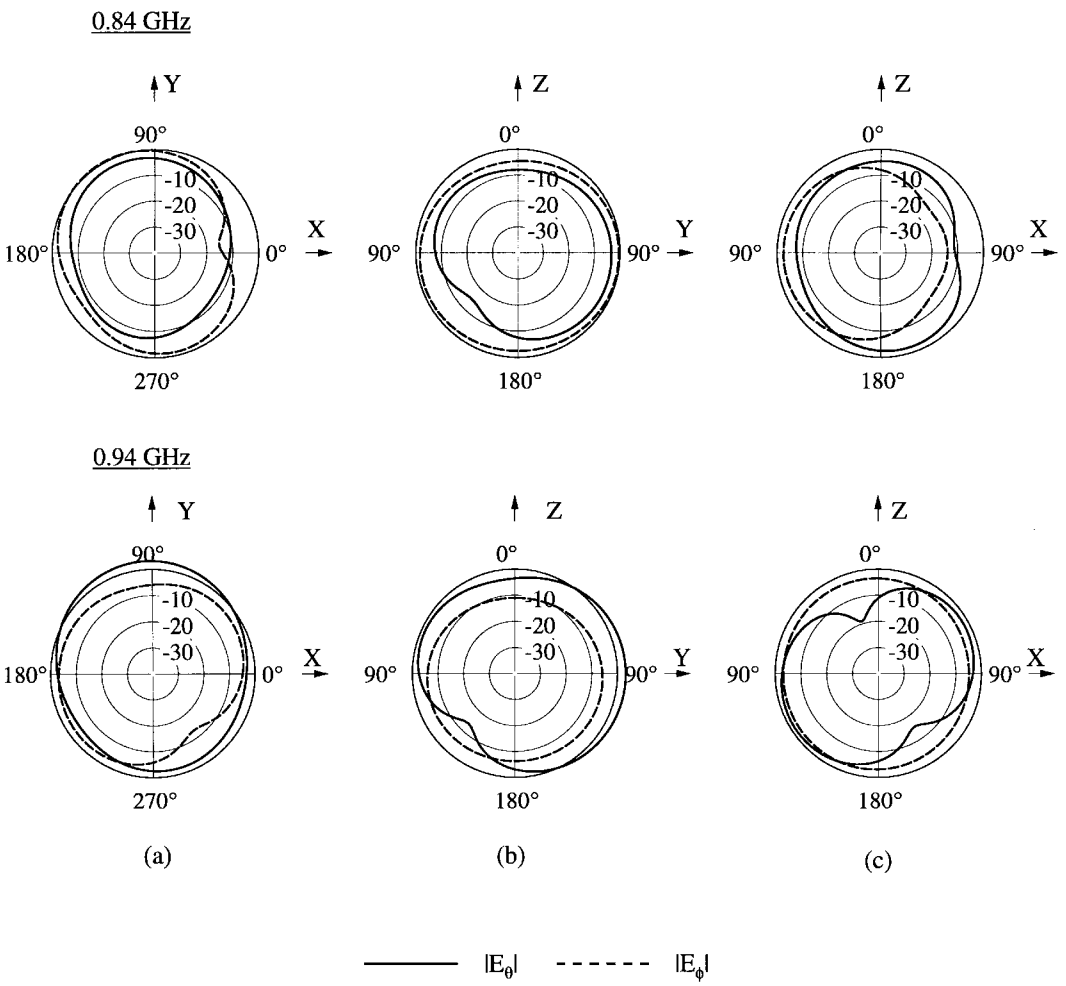


Fig. 12. Directivity patterns for Dual L antenna at 0.84 and 0.94 GHz for various far-field components. (a) $|E|$ dB versus $\phi$, $\theta = 90^\circ$, (b) $|E|$ dB versus $\theta$, $\phi = 90^\circ$, (c) $|E|$ dB versus $\theta$, $\phi = 0^\circ$.

Fig. 11 shows the magnitude of the surface currents for the Dual L antenna at 0.84 and 0.94 GHz. The main-fed element is the element on the right. A comparison of these plots shows that the distribution of the surface current magnitude is similar on both the main-fed and coupled elements at 0.84 GHz. This characteristic changes noticeably at 0.94 GHz. The surface current magnitude at 0.94 GHz is larger on the main-fed element than it is on the coupled element. This confirms the type of behavior exhibited in the study of input impedance. At the lower frequency, the surface currents and input impedance are determined by the geometry of the composite Dual L structure. At higher frequencies, the characteristics of the Dual L is determined primarily from the dimensions of the main-fed element.

The predicted directivity patterns for the Dual L antenna at 0.84 and 0.94 GHz are shown in Fig. 12. The antenna dimensions and coordinate system orientation are shown in Fig. 6. The directivity is computed using the antenna input voltage and current. The antenna has broad radiation patterns with both dominant $E_\theta$ and $E_\phi$ field components. The far-field patterns at 0.94 GHz resemble the patterns of an isolated PIFA element, while the patterns at 0.84 GHz do not. Fig. 11 shows that at 0.84 GHz there is strong interaction between the main-fed and coupled elements, which contributes to additional radiation of the electric field in the cross-polarized direction.

The design of the Dual L antenna begins with the design of the broadest bandwidth PIFA element. The starting Dual L is generated by placing an identical radiation-coupled element near the main-fed PIFA element. The gap between the two elements is determined so that the resistance between the resonance frequencies drops down to nearly 50 Ω. The length of the coupled element is then determined by finding the appropriate length in which the upper and lower resonances nearly combine.

### C. Diode-Tunable PIFA

The results of the study of the PIFA simulations show that the length of the top plate of the PIFA element is one dominant factor that controls the center frequency of operation. A mechanism that allows the length of the top plate to be varied electrically will result in a broad-band tunable low-profile antenna element.

The diode-tunable PIFA consists of a PIFA element that is divided into two sections, as shown in Fig. 13. Varactor

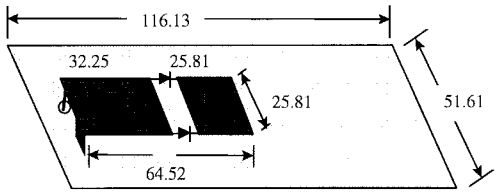


Fig. 13. Dimensions of diode-tunable PIFA. All dimensions are in millimeters.

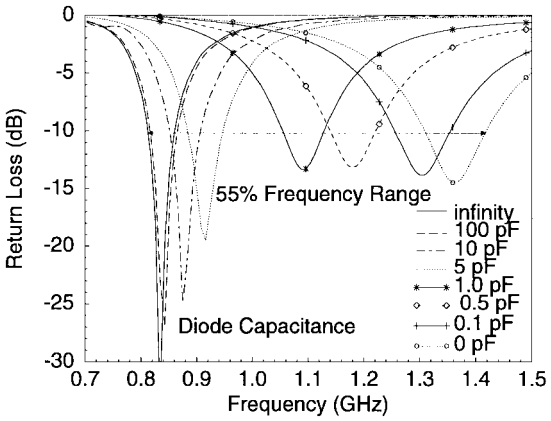


Fig. 14. Predicted return loss for ideal diode-tunable PIFA.

tuning diodes are located so they connect the two sections electrically together. The capacitance between the two sections is controlled by tuning the diodes, which effectively varies the electrical length, and thus the resonant frequency of the top plate. A computer program based upon the FDTD method was used for these simulations, since FDTD can easily handle lumped capacitive elements in the model. The MoM approach was initially used to assess the overall bandwidth achievable over the tuning range of the diodes for this antenna. The zero capacitance case can be modeled with the MoM by using two wires to connect the two parts of the top plate, while the infinity capacitance case is modeled by disconnecting the two parts of the top plate.

In order to obtain the greatest amount of tuning, the diodes are placed near the two side edges of the top plate, since the current is strongest near the edges. The particular division of the top plate element was determined from investigating the various points for which to split up the plate. Cases involving dividing the top plate near the end and dividing the top plate near the feed were considered. The predicted return loss for an ideal PIFA in which the capacitance of the diodes ranges from 0 to infinity, is shown in Fig. 14. The return loss for small capacitance values, even though not as low as the return loss when the capacitance is large, is lower than the 10-dB maximum return loss criteria. When based upon the VSWR less than 2:1 criteria, a 55% overall frequency band is achievable from this element.

Based upon the results of the simulations, a diode PIFA was fabricated from the dimensions specified in Fig. 13. The diode PIFA was fabricated in a manner similar to the PIFA. A small gap was etched into the top plate conductor in order to physically split the top plate conductor into two separate parts. Packaged beam-lead diodes were soldered across this

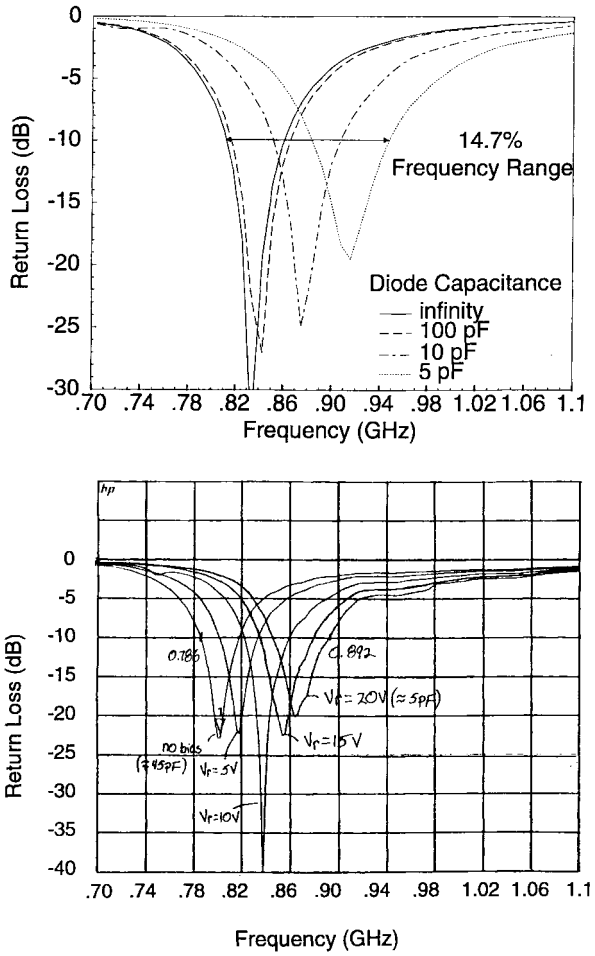


Fig. 15. Comparison of predicted and measured return loss for diode-tunable PIFA.

gap at the two edges of the top plate. Small inductors were also soldered near the diode beam leads. The inductors were used to isolate the RF signal currents on the top plate from the dc bias lines for the diodes.

Fig. 15 compares the predicted and measured return loss of the diode-tunable PIFA for the frequency range from 0.7 to 1.1 GHz. The actual diodes have capacitance ranging from 5 pF (for a 20-V reverse bias voltage) to 35 pF (for a 1.25-V reverse bias voltage). The results show how well the predicted and measured results compare and also show the overall tunability of the element. The frequency shift between the measured and predicted results is primarily due to the stray capacitance and inductance in the diode package and the bias circuitry. These parasitics were not included in the analysis model.

Currently available microwave tuning diodes do not allow capacitance tuning from zero to infinity. It is interesting to note that the greatest amount of tunability is obtained when small changes in small capacitance values are made. The maximum bandwidth of this element could be obtained if devices with this tuning range where utilized. The bandwidth of the element may also be further increased by shaping the gap between the two top plate sections and by tapering the top plate.

## IV. Summary and Conclusions

This paper has focused on the development of low-profile integrated antennas with enhanced bandwidth performance. The featured radiators have several advantages over other candidate antenna elements.

The results for the PIFA, radiation-coupled Dual L, and the diode-tunable PIFA show that these antennas are potential low-profile candidates for wireless communications systems. The PIFA can be designed for up to about 9.6% bandwidth. A Dual L antenna with a predicted bandwidth of 16% bandwidth and a diode PIFA antenna with 50% predicted bandwidth (considering ideal diodes) were designed. The design methodology to develop Dual L antennas for different frequencies of operation was described. Measured results on fabricated antennas were used to confirm the simulation results used FDTD and MoM. The measured results indicate that the resonant frequency of this class of antennas is sensitive to the location of the antenna feed. The visualization of the surface currents on the Dual L antenna was used to explain the antenna radiation characterization. The visualization of the currents for complex radiators on wireless packages is an excellent way to understand the interaction and performance of the antennas and the communications system.

The results and design details on the antennas presented here can be used as beginning designs for engineers interested in utilizing low-profile integrated antennas in new wireless communications systems.

## References


[1] A. Taflove, *Computational Electrodynamics: The Finite-Difference Time-Domain Method*. Norwood, MA: Artech House, 1995.

[2] M. A. Jensen and Y. Rahmat-Samii, "Performance analysis of antennas for hand-held transceivers using FDTD," *IEEE Trans. Antennas Propagat.*, vol. 42, pp. 1106–1113, Aug. 1994.

[3] S. M. Rao, D. R. Wilton, and A. W. Glisson, "Electromagnetic scattering by surfaces of arbitrary shape," *IEEE Trans. Antennas Propagat.*, vol. AP-30, pp. 409–418, May 1982.

[4] J. Rasinger, A. L. Scholtz, W. Pichler, and E. Bonek, "A new enhanced-bandwidth internal antenna for portable communication systems," in *Proc. 40th IEEE Veh. Technol. Conf.*, Orlando, FL, May 1990, pp. 7–12.

[5] K. Virga and Y. Rahmat-Samii, "An enhanced bandwidth integrated dual L antenna for mobile communications systems-design and measurement," in *IEEE Antennas Propagat. Symp. Dig.*, Newport Beach, CA, June 1995, pp. 1120–1123.

[6] ——, "Wide-band evaluation of communications antennas using $[Z]$ matrix interpolation with the method of moments," in *IEEE Antennas Propagat. Symp. Dig.*, Newport Beach, CA, June 1995, pp. 1262–1265.

[7] A. C. Ludwig, "Wire grid modeling of surfaces," *IEEE Trans. Antennas Propagat.*, vol. AP-35, pp. 1045–1048, Sept. 1987.

[8] K. S. H. Lee, L. Marin, and J. P. Castillo, "Limitations of wire grid modeling of a closed surface," *IEEE Trans. Electromagn. Compat.*, vol. EMC-18, pp. 123–129, Aug. 1976.

[9] J. S. Colburn and Y. Rahmat-Samii, "Electromagnetic scattering and radiation involving dielectric objects," *J. Electromagn. Waves Applicat.*, vol. 9, no. 10, pp. 1249–1277, 1995.

[10] R. E. Hodges and Y. Rahmat-Samii, "An iterative current-based hybrid method for complex structures," *IEEE Trans. Antennas Propagat.*, vol. 45, pp. 265–276, Feb. 1997.

[11] R. M. Fano, "Theoretical limitations on the broad-band matching of arbitrary impedances," *J. Franklin Inst.*, vol. 249, pp. 57–83, Jan. 1950.

[12] ——"Theoretical limitations on the broad-band matching of arbitrary impedances," *J. Franklin Inst.*, vol. 249, pp. 139–154, Feb. 1950.

[13] K. Hirasawa and M. Haneishi, *Analysis, Design, and Measurement of Small Low Profile Antennas*. Norwood, MA: Artech House, 1992.

[14] R. Luebbers, L. Chen, T. Uno, and S. Adachi, "FDTD calculations of radiation patterns, impedance, and gain for a monopole on a conducting box," *IEEE Trans. Antennas Propagat.*, vol. 40, pp. 1577–1583, Dec. 1992.

[15] M. A. Jensen and Y. Rahmat-Samii, "EM interaction of handset antennas and a human in personal communications," *Proc. IEEE*, vol. 83, pp. 7–17, Jan. 1995.


**Kathleen L. Virga** (S'84–M'85–SM'97) received the B.S. degree from California State University at Long Beach, in 1985, the M.S. degree from California State University at Northridge, in 1987, and the Ph.D. degree from the University of California at Los Angeles (UCLA), in 1996, all in electrical engineering.

From 1985 to 1996, she worked in the Radar Systems Group, Hughes Electronics, Electromagnetic Systems and Solid-State Microwave Laboratories. She has been a Task Leader and Supervisor for several internal research and development projects. She is currently an Assistant Professor in the Electrical and Computer Engineering Department, University of Arizona, Tucson. Her experience includes the design and development of phase shifters, RF feed networks, radiator elements, and transmit/receive modules for airborne phased-array and active array antennas, for which she holds four patents. Her research interests include personal communications, conformal antenna arrays, and the design and measurement of 3-D, high-density, high-speed digital and microwave circuits.

Dr. Virga is a member of Eta Kappa Nu, Tau Beta Pi, Sigma Xi, and the IEEE Antennas and Propagation (AP-S) and Microwave Theory and Techniques (MTT) Societies. She is the associate editor responsible for the PACE column for the AP-S *Magazine* and served on the Steering Committee which hosted the 1994 MTT International Microwave Symposium. In 1996, she was the second-place finalist in the USNC-URSI Student Paper Competition, and received the UCLA Department of Electrical Engineering Graduate Woman of the Year Award. She was the invited keynote speaker for the 1996 California State University Northridge, School of Engineering commencement.

**Yahya Rahmat-Samii** (S'73–M'75–SM'79–F'85) received the M.S. and Ph.D. degrees in electrical engineering from the University of Illinois, Urbana-Champaign.

He was a Senior Research Scientist at NASA's Jet Propulsion Laboratory/California Institute of Technology. In 1986, he was a Guest Professor at the Technical University of Denmark (TUD). He has also been a consultant to many aerospace companies. He is currently Professor of electrical engineering at the University of California at Los Angeles (UCLA). He has authored and co-authored over 380 technical journal articles and conference papers, has written thirteen book chapters, and is the co-author of *Impedance Boundary Conditions in Electromagentics*, published in 1995. He is also the holder of several patents. His research contributions cover a diverse area of electromagnetics, antennas, measurement and diagnostics techniques, numerical and asymptotic methods and satellite and personal communications.

Dr. Rahmat-Samii is a Fellow of IAE, a member of Commissions A, B, and J of USNC/URSI, AMTA, Sigma Xi, Eta Kappa Nu, and the Electromagnetics Academy. He was the 1995 President of IEEE Antennas and Propagation Society, and was appointed an IEEE Antennas and Propagation Society Distinguished Lecturer. He has been the guest and plenary session speaker at many national and international symposia, was one of the directors and vice president of the Antennas Measurement Techniques Association (AMTA) for three years, and was a member of UCLA's graduate council. He has been editor and guest editor of many technical journals and book publications. He has received numerous NASA and JPL Certificates of Recognition. In 1984, he was the recipient of the prestigious Henry Booker Award of URSI. In 1992 and 1995, he was the recipient of the Best Application Paper Award (Wheeler Award) for papers published in the IEEE Transactions on Antennas and Propagations. In 1993, 1994, and 1995, three of his Ph.D. students were named the Most Outstanding Ph.D. students at UCLA's School of Engineering and Applied Science and another received the Best Student Paper Award at the 1993 IEEE AP-Symposium. He is listed in *Who's Who in America*, *Who's Who in Frontiers of Science and Technology*, and *Who's Who in Engineering*.